Available online at www.sciencedirect.com
ScienceDirect
Polymer 47 (2006) 8536–8547
polymer
www.elsevier.com/locate/polymer

Preparation and properties of waterborne dual curable monomers and cured hybrid polymers for ink-jet applications

Chi-Jung Chang*, Haun-Yung Tzeng

Department of Chemical Engineering, Feng Chia University, 100 Wenhwa Road, Seatwen, Taichung 40724, Taiwan ROC

Received 3 March 2006; received in revised form 14 September 2006; accepted 7 October 2006
Available online 3 November 2006

Abstract

Linear and star-like waterborne UV/moisture curable monomers with surface activity were synthesized by introducing different amounts of trimethoxysilane and methacrylate units into the monomer chains. The surface morphology, transparency and thermal properties of the cured hybrid polymer were found to be determined by the monomer structure, solvent, the amount and arrangement of trimethoxysilane groups. The polymer–silica hybrid materials crosslinked with both UV curing and sol–gel reaction exhibited good thermal properties at elevated temperature. Due to the surface activity of monomers in aqueous medium, aggregates on the film made by water diluted monomers are larger than those prepared by solvent diluted monomers. Larger aggregates lead to lower transparency. Hybrid films made by star-like monomer had smaller silica aggregates than those prepared by the linear monomers. Star-like monomer exhibited excellent compatibility with water-based pigment dispersion and good ink-jet printing properties. It can be used to improve the properties of the ink-jet printed micropatterns.

Keywords: Hybrid material; Morphology; Dual curable

1. Introduction

The organic–inorganic nanocomposites can enhance the mechanical strength, thermal stability and flame retardance of the organic polymer [1–4]. The polymer–silica hybrid can be derived from the sol–gel process through the mixing of alkoxysilane compounds and polymer/curing agent together in a homogenous solution, followed by heating. During the heating period, the evaporation of solvent, the curing reaction of polymer, and the gelation reaction of the hydrolyzed alkoxysilane occurred simultaneously [5–8]. High inorganic contents have been introduced into the hybrid nanocomposites for the nano-scaled metal oxide particles [9]. The particles should be uniformly distributed within the hybrid material to achieve high specific surface areas of the nano-scaled particles and enhance mechanical properties of the hybrid material [10].

The color filter consists of repeatedly arranged tiny red (R), green (G) and blue (B) pixels. It is one of the important parts of the liquid crystal display. In this study, an environmental friendly process is developed by using the aqueous inks. A series of waterborne silylated moisture and UV dual curable monomers were prepared to be used in making the ink-jet printed color filter. The RGB pixels can be formed in a single step by ejecting the ink drops onto the color areas and fixing through curing reaction. The viscosity of the ink should be kept low to get good jetting properties at the frequency of more than 500 drops per second. In addition, curing reaction should effectively and instantaneously convert the liquid, low-viscosity formulation of ingredients into a polymerized solid polymer network.

The waterborne monomers can be prepared by modifying the hydrophobic backbone with built-in hydrophilic segments. Hydrophilic segments can be introduced by the incorporation of ionic groups, which can be anionic [11], cationic [12], or zwitterionic [13]. In this study, nonionic poly(ethylene glycol) segments were utilized as hydrophilic segments. The major

* Corresponding author. Tel.: +886 4 24517250x3678; fax: +886 4 24510890.
E-mail address: changcj@fcu.edu.tw (C.-J. Chang).

0032-3861/$ - see front matter © 2006 Elsevier Ltd. All rights reserved.
doi:10.1016/j.polymer.2006.10.012

limitation in using waterborne photocured monomers for printing micropatterns on non-absorbing substrates is the wetting character of these monomers before curing. It makes the cured pattern larger than the fresh-printed ones. Several efforts have been made to develop the barrier ribs around the micropatterns to improve this drawback [14–16]. However, the barrier rib prepared by the lithography process limits its processing convenience. Besides, our previous research [14] found that the competing absorption of the blue pigment hindered the thorough cure of the UV cured blue color strips. In addition, polymer films made by monomers with nonionic polyether segments such as poly(ethylene glycol) have poor thermal properties. To compete with color photoresists used in the conventional pigment dispersion method, the properties of waterborne monomers must be improved. The properties of the cured waterborne resin can be improved via grafting, crosslinking, and blending with other polymers. Many ways of crosslinking have been studied, including UV-crosslinking [17] and heat-activated [18] systems. To obviate the above mentioned problems, a secondary curing mechanism, such as curing by sol–gel reaction, is necessary [19]. Waterborne monomers combining both the photosensitive group and the moisture cure group in one molecule were synthesized in this study. Polymer/silica composites were obtained from the in situ curing of the silylated monomers. Adding the hybrid material might be a promising approach to obtain an ink-jet printed micropattern with good jetting precision and thermal properties.

This study discloses an approach for crosslinking the hydrophilic monomers and forming the micropatterns of ethoxylated polymer–silica hybrid materials on the non-absorbing glass substrates by ink-jet printing and sol–gel/UV curing processes. The influence of solvent, the silane-groups arrangement and silane content of monomers on the morphology and properties of the hybrid polymers were investigated. Consequently, these new hybrid materials show potentials in the applications of manufacturing color filter, microlens, and other display devices.

2. Experimental

2.1. Materials

Glycidyl methacrylate (TCI) and 2-hydroxy-2-methyl-1-phenyl-propan-1-one (Sartomer) were used as received. 1,4-Dioxane, polyoxyethylene (20) sorbitan monolaurate, 3-glycidoxypropyltrimethoxysilane, poly(ethylene glycol) methyl ether (average Mn ca. 750) and 1,2,4-benzenetricarboxylic anhydride (BTCA) were supplied by Aldrich Co. Star-like UV and moisture curable monomer (T20BG*m*T*n*, $m = 0-6$, $n = 0-6$, $m + n = 6$) was synthesized from polyoxyethylene (20) sorbitan monolaurate (Tween 20, T20) as the core molecule, 1,2,4-benzenetricarboxylic anhydride (BTCA) as an AB_2 monomer, 3-glycidoxypropyltrimethoxysilane (TGS), and glycidyl methacrylate (GMA) as the endgroup modifiers. By changing the feeding ratio of TGS and GMA, T20BG*m*T*n* was synthesized with *m* methacryloyl moieties and *n* trimethoxysilane moieties. Linear UV and moisture curable monomer (L7BG*m*T*n*, $m = 0-1$, $n = 0-1$, $m + n = 2$) was synthesized from poly(ethylene glycol) methyl ether (average Mn ca. 750, L7), 1,2,4-benzenetricarboxylic anhydride (BTCA), glycidyl methacrylate (GMA) and 3-glycidoxypropyltrimethoxysilane (TGS).

2.2. Synthesis of T20BG6

Polyoxyethylene (20) sorbitan monolaurate (2.45 g) was dissolved in DMF (10.85 g) in a three-necked flask. Then BTCA (1.15 g) was added into the flask. The flask was moved to an oil bath at 90 °C and stirred by a magnetic bar. The mixture was left to react for 8 h under nitrogen atmosphere. The heating temperature of the reaction mixture was kept at 70 °C. GMA (1.7 g) was dissolved in DMF (5.1 g) and then poured into the above mixture and reacted for 8 h under nitrogen atmosphere. The reaction scheme is shown in Scheme 1.

2.3. Synthesis of T20BGmTn and L7BGmTn

Similar procedures as mentioned in synthesizing T20BG6 were used for synthesizing T20BG*m*T*n* except replacing GMA by the mixture of GMA and TGS in the second step. For the synthesis of L7BG*m*T*n*, similar procedures as synthesizing T20BG*m*T*n* were used except replacing polyoxyethylene (20) sorbitan monolaurate by poly(ethylene glycol) methyl ether (Scheme 2).

2.4. Film formation

The films were prepared by coating the monomer solutions (25% in dioxane), followed by UV exposure and baking. After UV curing for 5 min, the film was heated stepwisely in vacuum oven (50 °C for 30 min, 100 °C for 30 min, 150 °C for 30 °C min, 170 for 30 min). For the water diluted monomer, the dioxane/water weight ratio is 1. The cured films were used for measuring the SEM, AFM images and UV–vis spectra.

2.5. Ink preparation

Diblock copolymer dispersants DB2 (styrene/AA ratio = 1.5) were synthesized according to our previous study [14] and used as dispersants. Pigment Red 149, Pigment Green 36 and Pigment Blue 60 were milled by DB2 polymer dispersants to prepare the pigment concentrates R01, G01 and B01, respectively.

The monomers (T20BG3T3 monomer (4 wt%), tetraethylene glycol diacrylate (4 wt%), ethoxylated(15) trimethylolpropane triacrylate (5 wt%)), 1,4-dioxane (4 wt%), initiator (1-hydroxy-2-methyl-1-propane-1-one, 1 wt%) and surfactant (Surfynol 465, Air Product co., 0.2 wt%) were stirred for 25 min. D.I. water (52 wt%) was then added and the mixture was stirred for 10 min. Finally, the pigment concentrate (30 wt%) was added and the mixture was stirred for 15 min

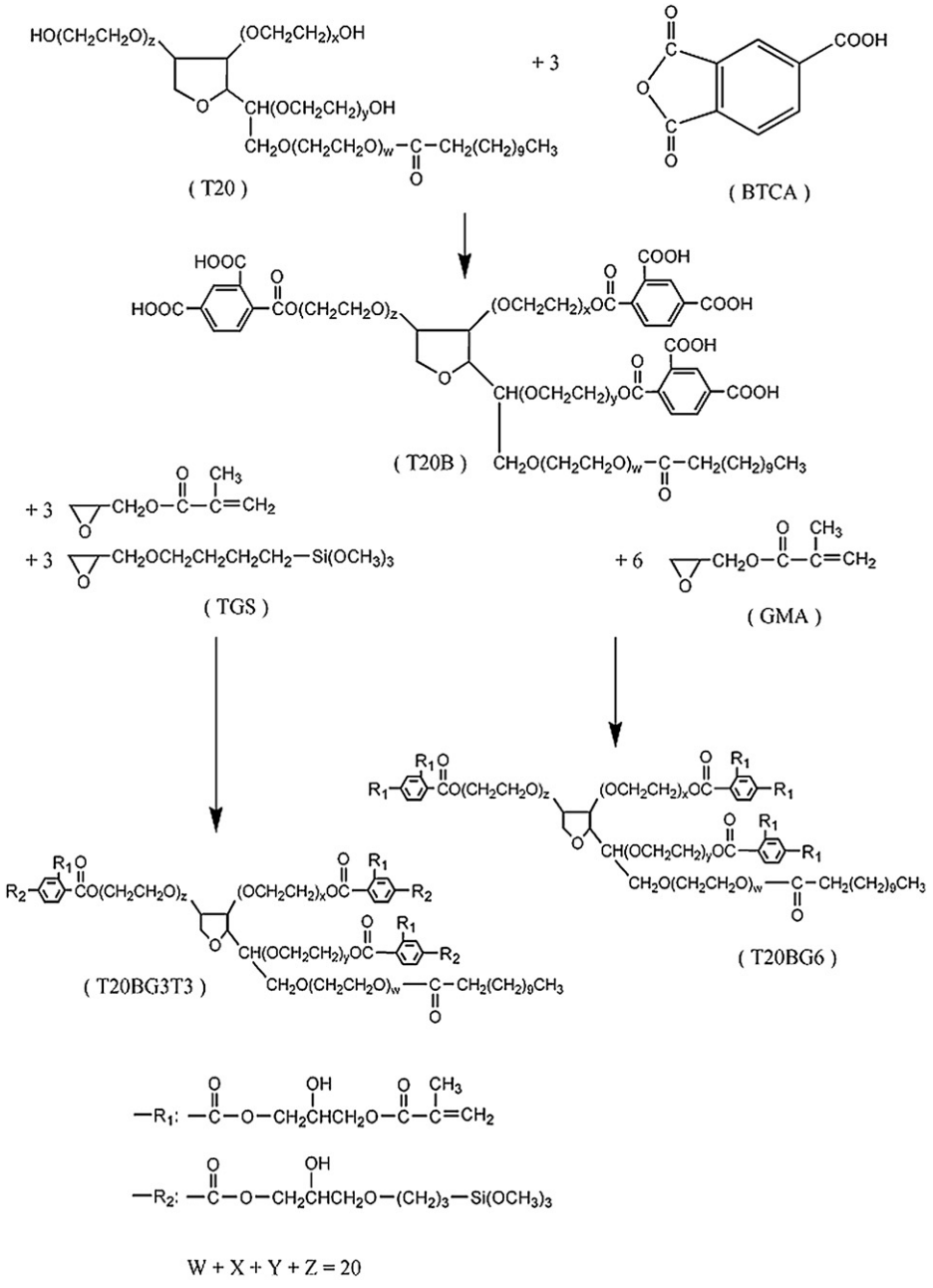

Scheme 1. Synthesis of T20BG6 and T20BG3T3.

to produce a UV/moisture dual curable ink-jet inks. The pigment concentrates R01, G01 and B01 were used to prepare the RH01, GH01 and BH01 inks, respectively.

2.6. Jetting properties

All the jetting properties were measured by the high-speed image capture system as shown in our previous study [20]. Signal control device was used to adjust the flashing signal of the LED and the operating parameters of the cartridge, such as the applied voltage, pulse width, firing frequency, and delay time. The delay time was the time interval between the pulse signal and the image capture operations. If the delay time was set at 50 μs, an image was captured after the drop was ejected for 50 μs. Inks were filled into the IUT626 cartridges and continuously jetted. The firing conditions were as listed below: pulse width 2.3 μs, driving voltage 17.8 V and firing frequency 500 Hz.

2.7. Characterization

Transmission FTIR spectra were collected on the Shimadzu IR Prestige-21 spectrometer. ^{29}Si NMR spectra were recorded with a Bruker DSX400WB (400 MHz) NMR spectrometer. Thermogravimetric analysis (TGA) was carried out using a TGA2950 apparatus from TA Instruments at a scan rate of

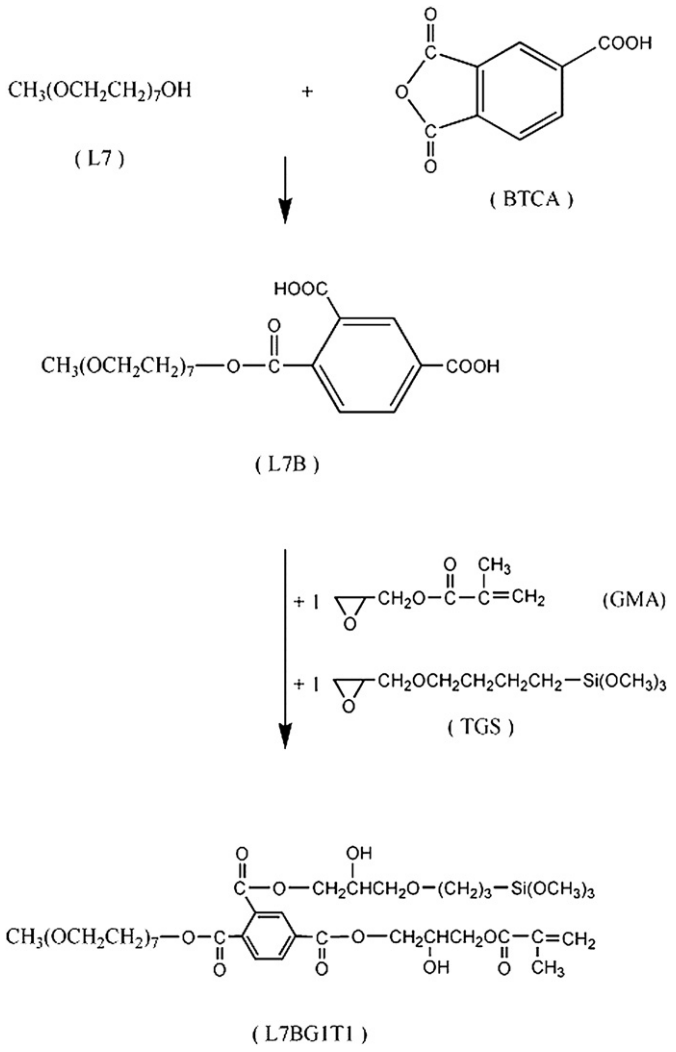

Scheme 2. Synthesis of L7BG1T1.

10 °C/min under nitrogen atmosphere. The absorbance and transmittance spectra of the nanocomposite coatings with 300–700 nm wavelengths were recorded by a UV–vis spectrophotometer (Hitachi UV-3000). Measurements of the surface tension were carried using a Kruss K6 Tensiometer. SEM measurements were conducted with a Hitachi S3000 variable vacuum scanning electron microscope and energy dispersive spectrometer. TEM experiments were carried out on a JEOL 1200 EX II with an accelerating voltage of 120 kV. AFM was performed with a multimode scanning microscope (NS4/D3100CL/MultiMode, Digital Instrument) in a tapping mode.

3. Results and discussion

The extent of reaction was monitored by the FTIR spectra of the reaction mixture. The IR spectrum of the reaction mixture of polyoxyethylene (20) sorbitan monolaurate and 1,2,4-benzenetricarboxylic anhydride is shown by curve (i) in Fig. 1. The absorption peaks at 1780 and 1850 cm^{-1} for anhydride groups of BTCA was disappeared after reacting at 90 °C

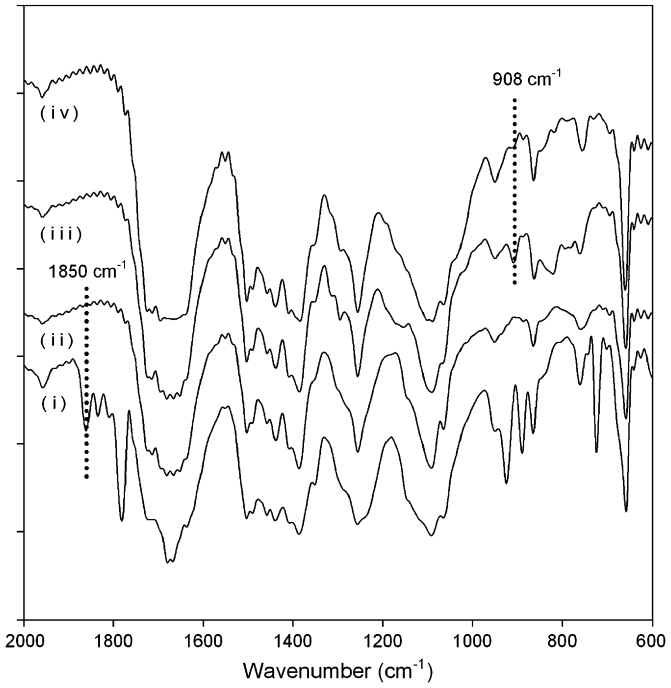

Fig. 1. FTIR spectra of (i) mixture of T20 and BTCA, (ii) T20B, (iii) mixture of T20B, GMA and TGS and (iv) T20BG3T3.

for 8 h under a nitrogen atmosphere, as shown in curve (ii). Then, the carboxylic acid group of polyolester reacted with glycidyl methacrylate and 3-glycidoxypropyltrimethoxysilane at 70 °C. The IR spectrum of the mixture of polyolester, glycidyl methacrylate and 3-glycidoxypropyltrimethoxysilane is shown in curve (iii). After reacting at 70 °C for 8 h under a nitrogen atmosphere, the absorption peak at 908 cm^{-1} (oxirane ring of GMA and TGS) was disappeared, as shown in curve (iv).

The typical FTIR spectra of T20BG3T3 before and after UV irradiation are illustrated in Fig. 2. Methacryloyl and trimethoxysilane moieties are present in each terminal group of the branched chain. The peak at 1635 cm^{-1} is separated from the other peaks, it is used to quantify the conversion of C=C bonds in UV-curable coatings, with the peak at 1725 cm^{-1} being due to C=O stretching absorbance as the reference for its invariability during UV curing [21]. The intensity of the peak at 1635 cm^{-1} for the C=C stretching vibration decreases with increasing exposure time under UV irradiation. The conversion of C=C bonds can be calculated according to the following equation:

$$\text{Conversion}\ (\%) = 100 \times (1 - A_t S_0 / A_0 S_t) \quad (1)$$

where A_t and A_0 are the areas of the peak at 1635 cm^{-1} and S_t and S_0 are the areas of the peak at 1725 cm^{-1} at an irradiation time t and $t = 0$, respectively. Based on the data calculated by Eq. (1), the conversion of T20BG3T3 and T20BG6 samples were 22.8% and 46.6%, respectively. The relative low conversion of C=C bonds of the former is possibly attributable to the hindered UV curing, which results from the decreased

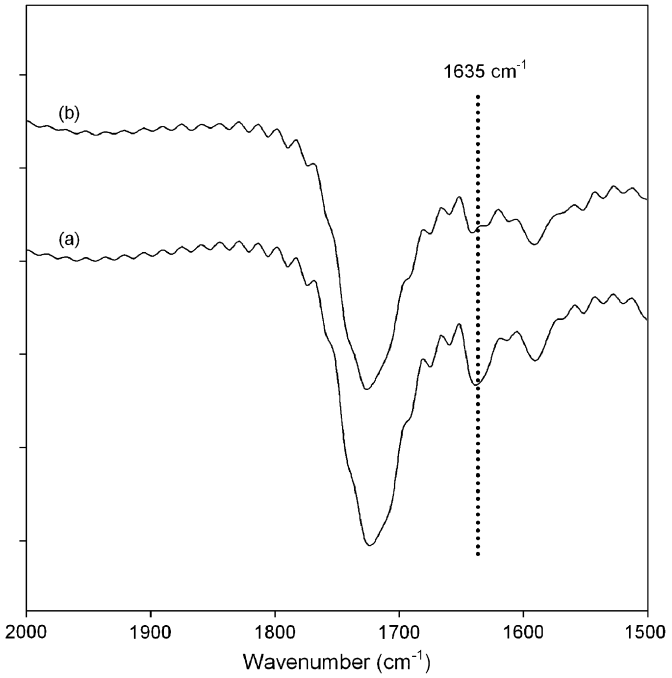

Fig. 2. FTIR spectra of T20BG3T3 (a) before and (b) after UV irradiation.

chain motion flexibility during the moisture curing reaction of trimethoxysilane moieties.

Fig. 3 shows the solid state ^{29}Si NMR CP-MAS spectra of cured T20BG3T3, T20BG1T5 and L7BG1T1 hybrid resins. The condensation reaction of the silanol groups and the structure of the silica formed were observed with solid state ^{29}Si NMR. The T signals originate from trialkoxysilane groups. The three peaks were assigned to the corresponding absorptions of dihydroxy-substituted silica (T^1, −50 ppm), monohydroxy-substituted silica (T^2, −58 ppm), and non-hydroxy-substituted silica (T^3, −66 ppm) [22]. It demonstrated the existence of the Si−O−Si structure in the samples. The total amount of siloxane bridges was used to evaluate the condensation degree of the condensed silica [23]. To illustrate the silica structures formed in the hybrid films, the peak integration data were summarized in Table 1 by setting the deconvolution assignments at −50 (T^1), −58 (T^2) and −66 ppm (T^3). For the T20 series film, the calculated conversions of the Si−OH condensation reactions in the hybrid films increased with increasing the TGS contents. T20BG1T5 film displayed a more condensed silicate structure (conversion = 77.6%) than that of the T20BG3T3 film. T^2 was the majority species in both films, but the former contained more T^3 (40.7%) than the latter (25.9%). L7BG1T1 is a linear monomer and contains similar TGS content (25 wt%) with star-like T20BG3T3 monomer (24 wt%). However, cured L7BG1T1 film exhibited a less condensed silicate structure (conversion = 64.1%, T^3: 18%) than that of the T20BG3T3 film (conversion = 69.6%, T^3: 25.9%). It revealed that both the structure and TGS content of the monomers affected the conversion of the condensation reaction and the SiO_2 structure of the cured hybrid films.

Since silica was formed by the sol−gel reaction of the silane groups on adjacent monomers. Monomers with different silane group arrangement may have different influences on the morphology and properties of UV-curable composites with silica. The influence of the silane-groups arrangement

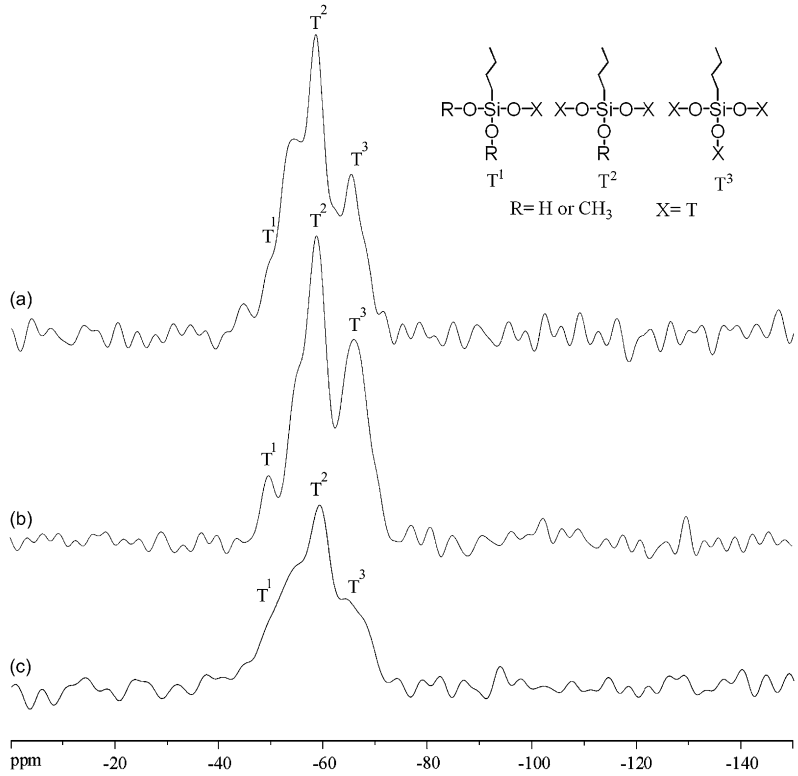

Fig. 3. ^{29}Si NMR CP-MAS spectra of cured (a) T20BG3T3, (b) T20BG1T5 and (c) L7BG1T1.

Table 1
Silica structure and condensation conversion data for the hybrid polymers from ^{29}Si NMR analysis

Sample	TGS content (wt%)	Composition of silanol structure (%)			Conversion (%)
		T^1	T^2	T^3	
T20BG3T3	24	17.0	57.1	25.9	69.6
T20BG1T5	37	8.0	51.3	40.7	77.6
L7BG1T1	25	25.8	56.2	18.0	64.1

Conversion (%) = $(T_1 \times 1 + T_2 \times 2 + T_3 \times 3)/3$.

and silane content of the monomers on the morphology and properties of UV cured hybrid film was investigated.

The topographic AFM images of T20BG3T3 and L7BG1T1 films made by dioxane diluted monomers are shown in Fig. 4(a) and 4(b), respectively. T20BG3T3 monomer has the hydrophilic furan ring centers, radially extended polyethylene oxide chains, and endcapped with hydrophobic acrylate and silane groups. The surface of T20BG3T3 film consists of many well-distributed small bulges and some large aggregates. The diameter of the aggregate was about 250–450 nm. L7BG1T1 is a linear monomer with hydrophilic polyethylene oxide chains at one side and hydrophobic acrylate and silane chains at the other side. Let S/A/E represented the weight ratio of silane groups/acrylate groups/ethylene oxide repeating unit. T20BG3T3 and L7BG1T1 had similar S/A/E ratio. That is, the T20BG3T3 and L7BG1T1 molecules had similar hydrophilic/hydrophobic segments ratio. There are many flake-like aggregates on the surface of the cured L7BG1T1 film. However, when the monomers were diluted by a mixture of water and dioxane, the linear and star-like monomers lead to cured films with different morphology. There are many aggregates with diameters of 100–400 nm for the film made by water diluted T20BG3T3 monomer. The aggregate size was about the same as those prepared by solvent diluted monomers. However, the AFM topography of films prepared by water diluted L7BG1T1 monomer (Fig. 4(c)) showed large aggregates with diameter of about 5 μm. These moisture and UV-curable monomers can be used in the application of waterborne coatings. Since these monomers have hydrophobic and hydrophilic segments, they may act as surfactants in aqueous solutions. As shown in Fig. 5, their analogs (T20BG6 and L7BG2) with acrylate ends exhibited surface activity. The lowering of the water surface tension and the micelle formation clearly revealed the amphiphilic character of these monomers. Yu et al. [24] found that the fluorinated alkyl side chains of the fluorinated polymethacrylate were found to orient toward the surface. The self-migration and orientation of the fluorinated polymer chains lead to the special topography of the fluorinated PUA film. We expected that films made by water diluted monomers might exhibit different surface morphology because of the surface activity of monomers. In addition, incorporation of water can promote the sol–gel reaction of the water diluted monomer and may also contribute to the larger aggregation size than that of the organic solvent based solution.

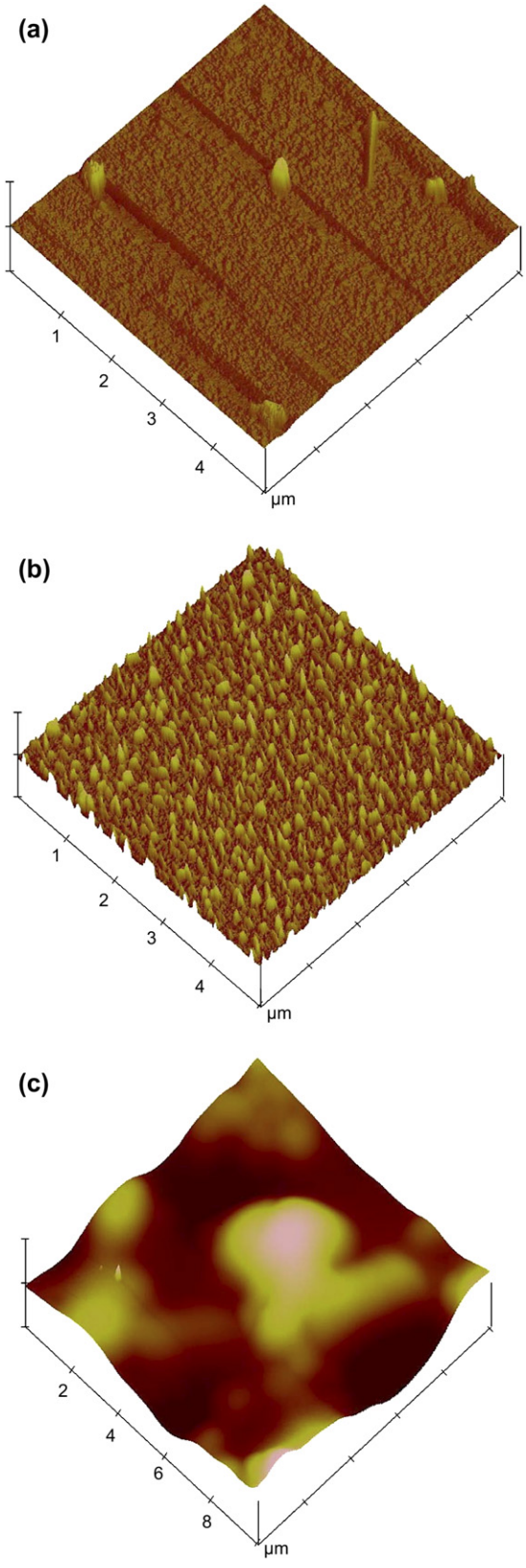

Fig. 4. Topographic AFM images of cured (a) T20BG3T3, (b) L7BG1T1 films made by dioxane diluted monomers and (c) L7BG1T1 film made by water/dioxane diluted monomers.

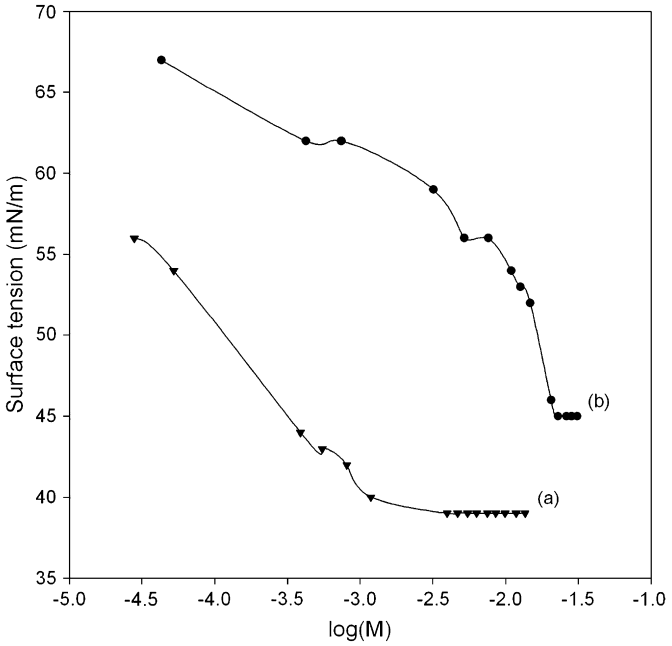

Fig. 5. Surface tension of (a) star-like T20BG6 and (b) linear L7BG2 monomers at different concentrations.

The SEM images of the cured films are shown in Fig. 6. There were particles with diameters of 400–500 nm on films made by dioxane diluted T20BG3T3 (Fig. 6(a)). The size of the particle on the film made by dioxane diluted L7BG1T1 was about 500 nm (Fig. 6(b)). Similar results were observed on films made by water/dioxane diluted T20BG3T3 monomer. Fig. 6(c) shows the SEM image of films prepared by water/dioxane diluted L7BG1T1 monomer. Large aggregates with diameter of about 3–5 μm were observed on the film made by water diluted linear monomer. The results of the film surface morphology agreed with those observed by the AFM (Fig. 5).

The TEM images of thin slices of hybrid films shown in Fig. 7 offered more details about the texture of the aggregates. Aggregates with various size and shape were observed for different hybrid films. Films made by dioxane diluted T20BG3T3 monomers had aggregates ranged from 200 to 400 nm (Fig. 7(a)). The aggregates consisted of many small tiny particles. Films made by dioxane diluted L7BG1T1 monomers (Fig. 7(b)) also had aggregates with similar size and texture as those shown in Fig. 7(a). For the cured films made by water/dioxane diluted T20BG3T3 monomer, the size of the aggregate was about 500 nm (Fig. 7(c)). However, for the cured films made by water/dioxane diluted L7BG1T1 monomer (Fig. 7(d)), the size of the aggregate was much larger (3.5 μm) and the structure was more compact than that of the films made by dioxane diluted L7BG1T1 (Fig. 7(b)). Incorporation of water can promote the sol–gel reaction and may also contribute to the larger aggregates and more compact structure.

Since the results of AFM, SEM and TEM revealed that addition of water had different influences on the linear L7BG1T1 and star-like T20BG3T3 monomers, we propose that surface activity may play a role on the morphology of the cured films. A schematic model for the formation of micelles in aqueous solution and the large aggregates on the film made by water diluted L7BG1T1 monomer after UV curing and sol–gel reaction is proposed and shown in Fig. 8. In the aqueous solution, the monomer might form micelles with the ethylene oxide segments stretched toward the water medium and the hydrophobic acrylate and silane segments located inside the

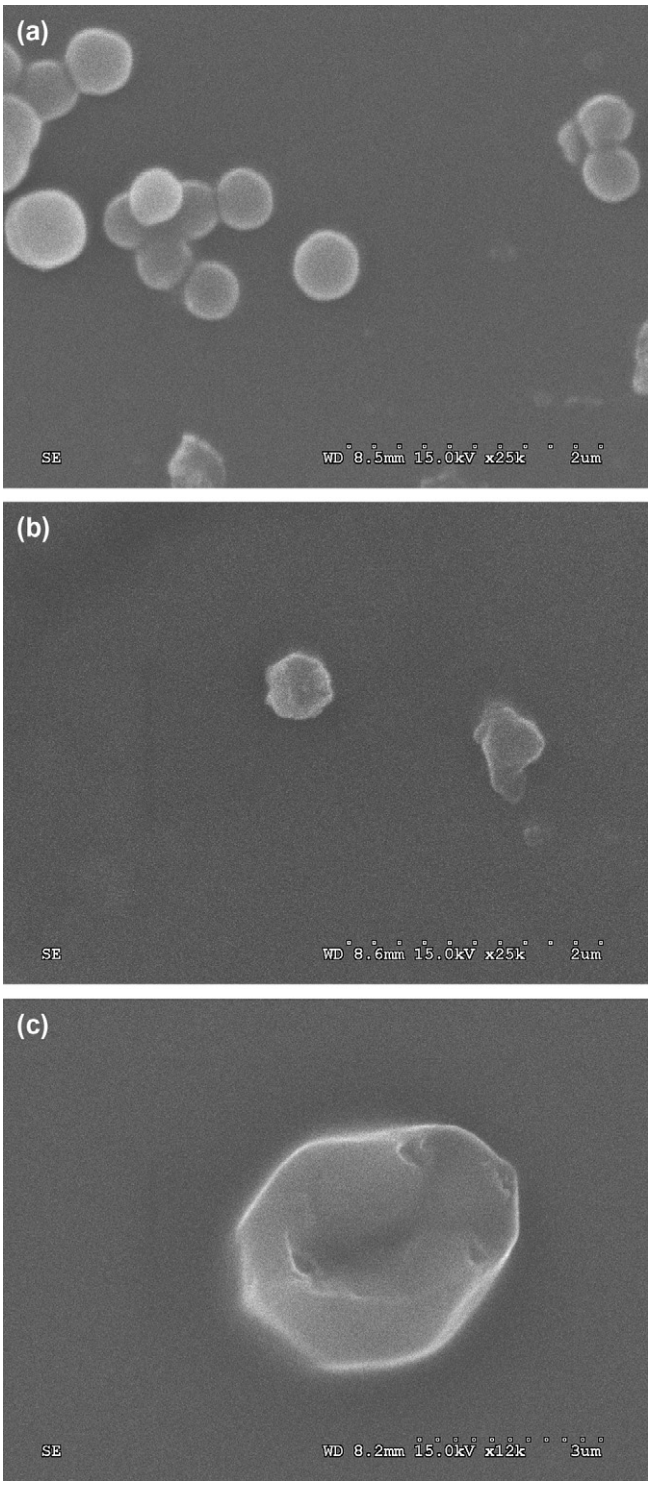

Fig. 6. SEM images of cured (a) T20BG3T3, (b) L7BG1T1 films made by dioxane diluted monomers and (c) L7BG1T1 films made by water/dioxane diluted monomers.

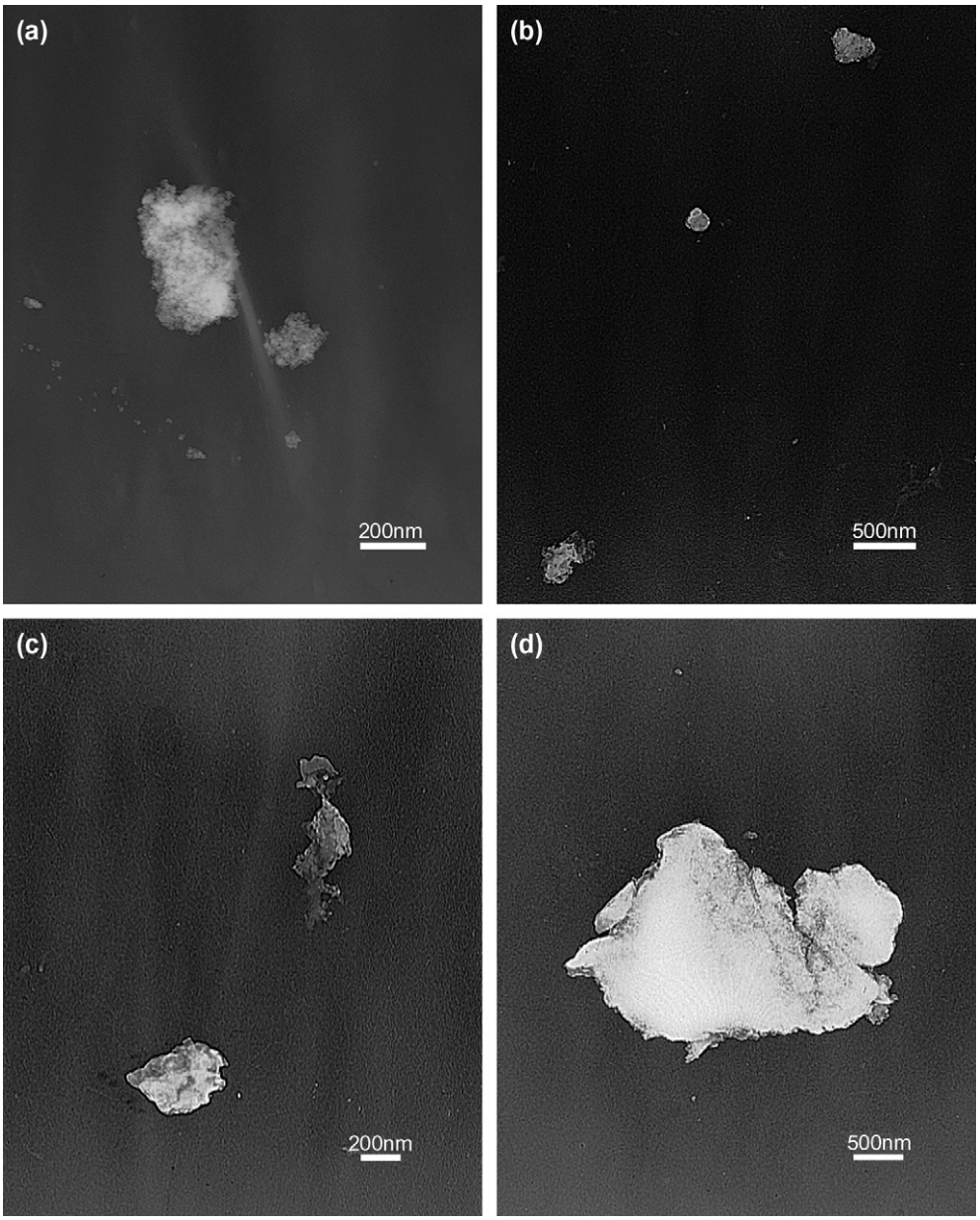

Fig. 7. TEM images of cured (a) T20BG3T3, (b) L7BG1T1 films made by dioxane diluted monomers and (c) T20BG3T3, (d) L7BG1T1 films made by water/dioxane diluted monomers.

micelle. After UV light exposure, there are several covalent bonds connecting the monomers within the micelles. Then, the condensed silica cluster was formed within the micelles by the sol–gel reaction of silane groups during baking. That is why the aggregates on the film made by water diluted L7BG1T1 monomer are larger than those prepared by the solvent diluted monomer. T20BG3T3 monomer has the hydrophilic centers and radially extended hydrophobic chains. L7BG1T1 is a linear monomer with hydrophilic chains at one side and hydrophobic chains at the other side. The experimental results showed that the linear structure favored the formation of larger micelles in the aqueous environment.

The optical properties of hybrid composites are critical to their application in some fields such as color filter, optical fiber coatings, lens coatings, and so forth. Fig. 9 illustrates the UV–vis spectra of the hybrid composite coatings. T20BG1T5 and T20BG3T3 films showed higher transparency than T20BG6 film. In the range of 400–700 nm wavelengths, more than 90% transmittance for T20BG1T5 and T20BG3T3 films prepared by solvent diluted monomers was observed. The high transparency implied that there was no macro-phase separation occurring in the films made by solvent diluted monomers. It agreed with the AFM results. However, larger differences occurred between films made by water diluted monomers and those prepared by solvent diluted monomers. The former exhibited larger decrease in the transmittance than the latter. The low transparency implied that there was large aggregation occurring in the films prepared by water diluted monomers. The results from AFM, SEM and TEM support the above mentioned explanation.

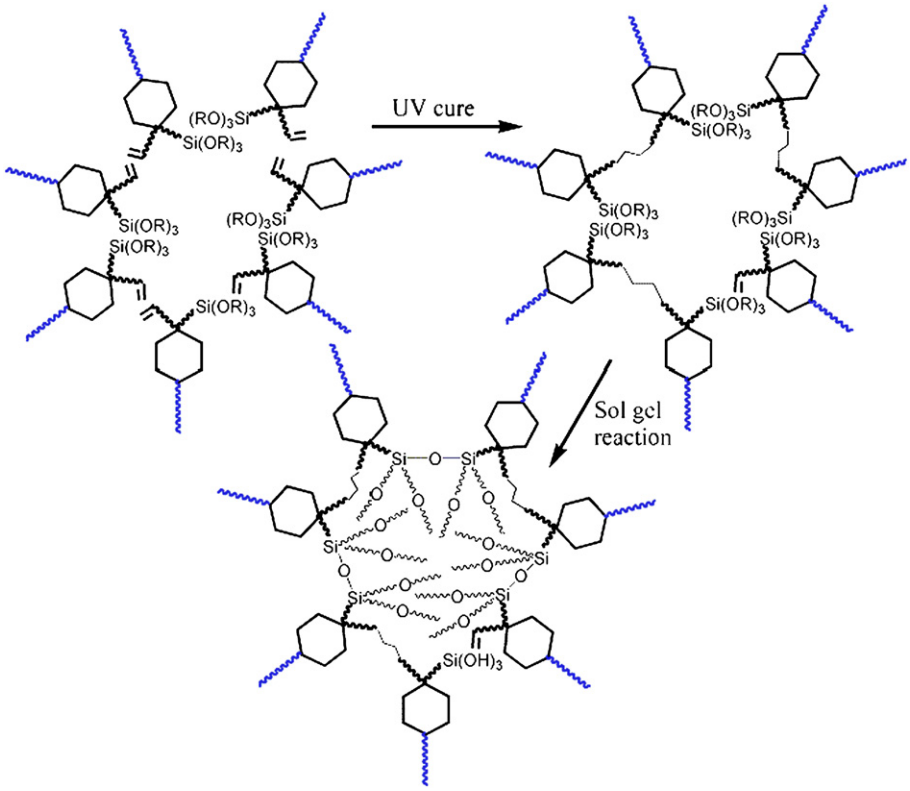

Fig. 8. Schematic model for the formation of micelles in aqueous solution and the large aggregates on the film made by water diluted L7BG1T1 monomer after UV curing and sol–gel reaction.

T20BG3T3 and other ingredients were used to prepare the RH01, GH01 and BH01 inks according to the procedures illustrated in Section 2. The UV–vis spectra of the cured red (RH01), green (GH01) and blue (BH01) color film are shown in Fig. 10. Compared with our previous study, all films showed good transparency.

The waterborne monomers were prepared by modifying the hydrophobic backbone with built-in hydrophilic poly(ethylene

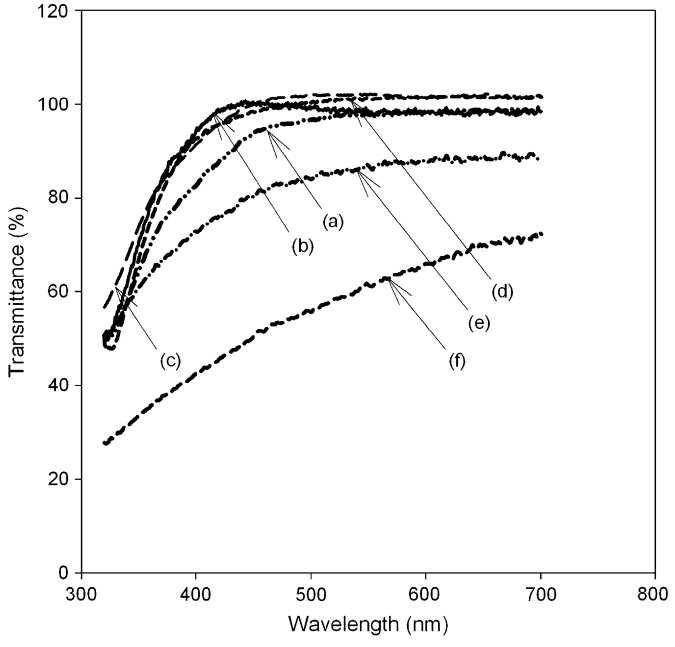

Fig. 9. UV–vis spectra of (a) T20BG, (b) T20BG3T3, (c) T20BG1T5, (d) L7BG1T1 films made by solvent diluted monomers and (e) T20BG3T3, (f) L7BG1T1 films made by water diluted monomers.

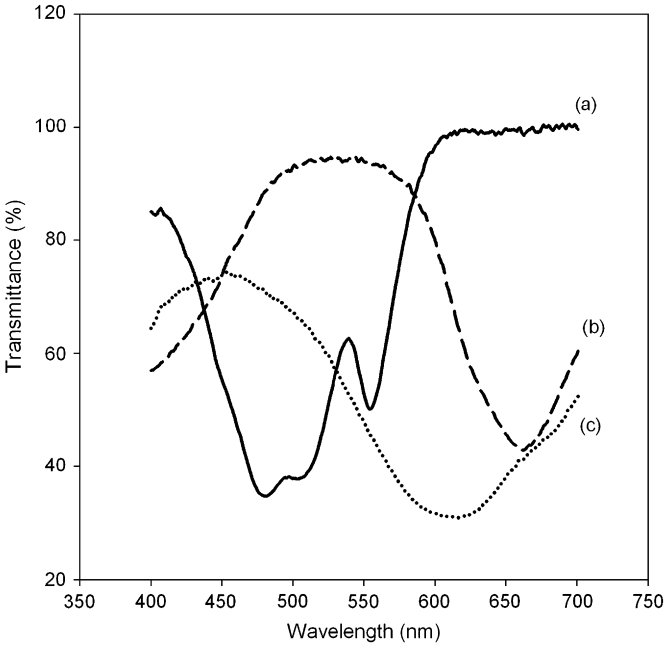

Fig. 10. UV–vis spectra of the cured (a) red (RH01), (b) green (GH01) and (c) blue (BH01) color films containing T20BG3T3.

Table 2
Thermal properties of the cured and hybrid polymers in nitrogen

Sample	TGS content (wt%)	Solvent for dilution	Thermal stability[a] (°C)	Td[b] (°C)	Char yield at 700 °C (%)
T20BG6	0	Dioxane	160	218	0
T20BG3T3	24	Dioxane	215	280	7.1
T20BG1T5	37	Dioxane	215	280	15.7
L7BG1T1	25	Dioxane	250	290	15.7
T20BG3T3	24	Water and dioxane	250	290	8.6
L7BG1T1	25	Water and dioxane	250	302	10.0

[a] Temperature at the onset point of weight loss.
[b] Temperature at 10% weight loss.

glycol) segments. However, polymer films made by monomers with poly(ethylene glycol) have poor thermal properties. The thermal stability and degradation behavior of the T20BG6, T20BG3T3 and T20BG1T5 samples were evaluated by TGA under nitrogen atmosphere. Pure polymer exhibited a weight loss starting at about 160 °C and a rapid weight loss at 200–300 °C. Taking the temperature at 10% weight loss (Td) to evaluate the thermal stability of the hybrid materials, it can be seen that polymer–silica hybrids exhibited better thermal stability than that of the pure polymer did. The temperatures of rapid weight loss of the cured T20BG1T5 sample also shifted to higher temperature regions. In addition, formation of polymer–silica hybrid materials also increased the char yields of the polymers at high temperatures. The increase in char yields resulted from the formation of thermally stable silica. The formed silica showed excellent thermo-oxidative stability to provide a retarding effect on the thermal degradation of the organic component of the hybrids and to enhance the heat resistance of the hybrid resins. Yu et al. [25] reported that silica network formed from sol–gel reaction of alkoxysilane compounds might penetrate into the PMMA chains. A barrier layer was formed to retard the degradation of the polymer domain and increase the char yields. Comparing the effects of TGS content, cured T20BG1T5 sample with higher TGS contents showed similar initial weight loss and fast weight loss curve with that of the T20BG3T3 sample. However, as shown in Table 2, the char formation of the hybrids was enhanced with incorporation of the silane groups, and increased with increasing silane-groups content. Compared with hybrid polymers made by solvent diluted monomers, the hybrid polymers made by water diluted monomers exhibited higher Td, but the char yield was lower. It was due to the higher thermal stability of the siloxane bond and crosslinking density of the silylated hybrid polymer, together with the formation of covalent bonding between the inorganic silica and organic polymer domain. It indicated that the large aggregates shown in Fig. 4 consisted of a tethered structure of organic regions and microstructured siloxane networks. The tethered structure of the large aggregate may retard the degradation before 500 °C. But the effect of retardation diminished at higher temperatures.

UV-curable jet inks were ejected onto the glass substrate and fixed by UV curing reaction to prepare LCD color filter. Poor directionality of jetting drops and non-uniform drop size may cause color filter defects such as blank areas in the color stripes and error dots lying in the neighboring stripes. The jetted drops should be precisely controlled to prevent the above mentioned defects. It is important to check the influence of different compositions on the jetting performance. Fig. 11 illustrates the drop formation images of GD01 inks

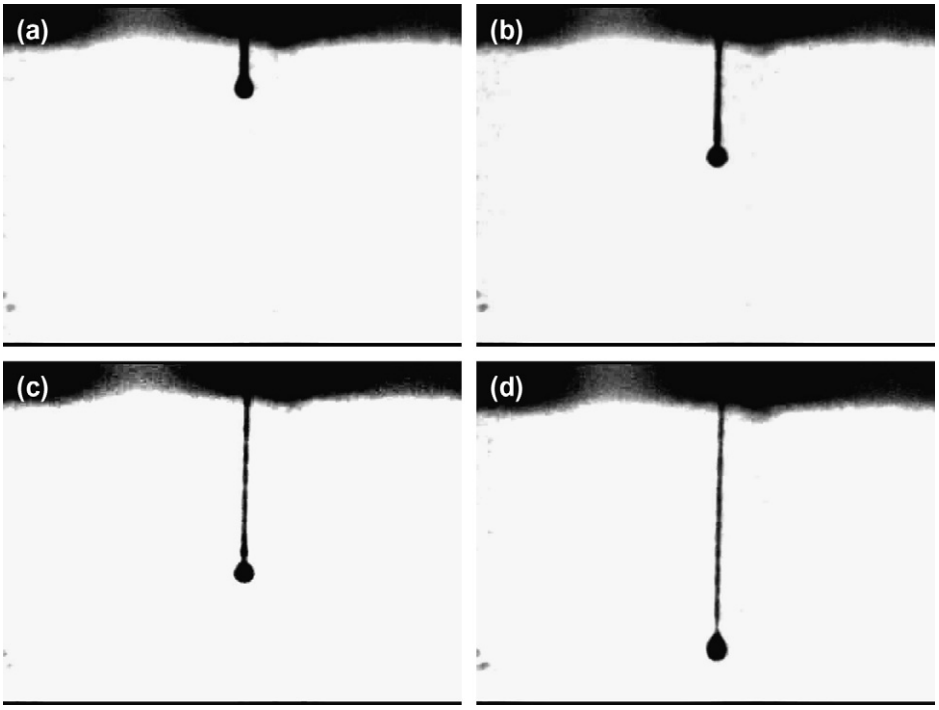

Fig. 11. Drop formation images of the GH01 ink captured at different delay times: (a) 50 μs (b) 70 μs (c) 80 μs (d) 100 μs.

captured at different delay times. The delay time is the time interval between the pulse signal and the image capture operation. Jetting directionality and stability are important for preparing the color filter via the ink-jet method. Inks were filled into the thermal bubble type (IUT51626) cartridges and continuously jetted. The firing conditions were as follows: pulse width 2.2 μs, driving voltage 17.8 V, and firing frequency 500 Hz. The ink droplet of GD01 ink exhibited uniform drops and straight trajectory. It revealed that incorporation of some silylated monomers in the ink will not deteriorate the jet printing properties of the ink solution.

The optimal printing parameters, such as the number of ink drops to be ejected within a certain distance is important for manufacturing the ink-jet printed color filter. A test pattern consisting of the dot array was utilized to compare the jetting trajectory and drop size uniformity. The jetting trajectory can be checked by the alignment of different dots, while the drop size uniformity can be analyzed by the size of printed dots. The ink was printed on the transparency film (3M PP2900), which did not included any ink-absorption layer. As shown in Fig. 12(a), there were some tiny holes on the 3M PP2900 transparency film. The diameters of the tiny holes were generally less than 10 μm and randomly distributed. As shown in Fig. 12(b), the printed dots were larger and aligned in the green dot-array. Each printed dot was formed by a single ink drop ejected from a single nozzle. Since the 3M PP2900 transparency film did not included any ink-absorption layer, the ink droplets were fixed with moisture curing and UV curing. The printer head moved in the horizontal direction. Meanwhile, the transparency film was fed in the vertical direction. The GD01 ink displayed good directionality in the horizontal direction, but a little bit poorer in the vertical direction. The average dot size is about 98 μm. The dot size of the test pattern is even smaller than that in our previous study [16] (113–116 μm) which were made by printing aqueous UV-curable inks on 3M CG3460 transparency film. In this study, the ink contained UV/sol–gel curable monomers and the substrate is non-absorbing transparency film. On the contrary, the ink contained only UV-curable monomers and the substrate is transparency film with an ink-absorbing layer in our previous study [16]. The ink was absorbed by the absorbing layer after printing. The difference in dot size between these experiments revealed that incorporating UV/sol–gel curable monomers as ink ingredients helped to fix printing patterns on non-absorbing substrate and increase the printing resolution (smaller dot).

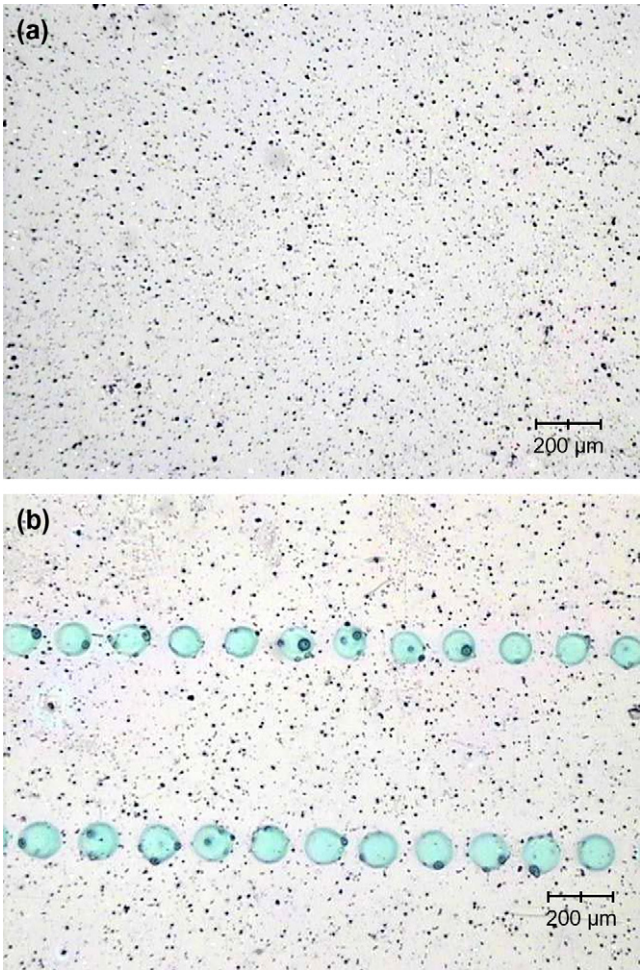

Fig. 12. (a) Surface of the blank 3M PP2900 transparency and (b) ink-jet printed dot arrays of GH01 green ink on 3M PP2900 transparency.

4. Conclusions

The NMR spectra showed that waterborne organosilane segments hydrolyzed to form silica particles. The organic–inorganic hybrid films showed better thermal stability at elevated temperature than its polymeric analog did, probably because of the higher thermal stability of the siloxane bond and crosslinking density of the hybrid polymer. Due to the surface activity of monomers in aqueous medium, films made by different monomer solutions resulted in different surface morphology. Aggregates on the films made by water diluted monomers are larger than those prepared by solvent diluted monomers. Larger aggregates lead to lower transparency. The optical properties of nanocomposites are critical in optical applications such as color filter, optical fiber coatings, and lens coatings. Hybrid films made by star-like monomer had smaller silica aggregates and higher transparency than those prepared by the linear monomers. Star-like monomer exhibited good compatibility with water-based pigment dispersions and good ink-jet printing properties. No pigment aggregation problems were observed. Organic–inorganic nanocomposite hybrid micropatterns were prepared through the ink-jet printing and a dual-cure process involving photopolymerization and condensation reactions of star-like monomer. It can be used to improve the properties of the ink-jet printed micropatterns.

Acknowledgements

The authors would like to thank the financial support from National Science Council under the contract of NSC-93-2218-E-035-011.

References

[1] Tyan HL, Leu CM, Wei KH. Chem Mater 2001;13:222.
[2] Zhu J, Morgan AB, Lamelas FJ, Wikkie CA. Chem Mater 2001;13:3774.
[3] Chen WJ, Lee SJ. Polym J 2000;32:67.
[4] Yeh JM, Liou SJ, Lin CY, Cheng CY, Chang YW, Lee KR. Chem Mater 2002;14:154.
[5] Kang S, Hong SI, Choe CR, Park M, Rim S, Kim J. Polymer 2001; 42:879.
[6] Schmidt H. Mater Res Soc Symp Proc 1990;171:3.
[7] Matejka L, Dusek K, Plestil J, Kriz J, Lednicky F. Polymer 1998;40:171.
[8] Ochi M, Takahashi R, Terauchi A. Polymer 2001;42:5151.
[9] Dang TD, Chen JP, Arnold FE. Hybrid Organic–Inorganic Composites. In: Mark JE, Lee CYC, Bianconi PA, editors. ACS Symposium Series 585. Washington, DC: American Chemical Society; 1995 [chapter 21].
[10] Nakamura Y, Yamaguchi M, Iko K, Okubo M, Matsumoto T. J Appl Polym Sci 1992;45:2066.
[11] Lorenz O, Hick H. Angew Makromol Chem 1978;72:115.
[12] Chan WC, Chen SA. Polymer 1988;29:1995.
[13] Yang CZ, Hwang KKS, Cooper SL. Macromol Chem 1983;184:651.
[14] Chang CJ, Shih KC, Chang SJ, Wu FM, Pan FL. J Polym Sci Polym Phys 2005;43:3337.
[15] Chang CJ, Chang SJ, Wu FM, Hsu MW, Chiu WW, Cheng K. Jpn J Appl Phys 2004;43:8227.
[16] Chang CJ, Wu FM, Chang SJ, Hsu MW. Jpn J Appl Phys 2004;43:6280.
[17] Kim HD, Kim TW. J Appl Polym Sci 1998;67:2153.
[18] Tirpak RE, Markusch PH. J Coat Technol 1986;58:49.
[19] Yamamura T, Watanabe T, Takeuchi A. Ukachi T. U.S. Patent 6,365,644, 2002.
[20] Chang CJ, Chang SJ, Tsou S, Chen SI, Wu FM, Hsu MW. J Polym Sci Polym Phys 2003;41:1909.
[21] Li F, Zhou S, Wu L. J Appl Polym Sci 2005;98:1119.
[22] El-Sayed M, Seifert A, Spange S. J Sol Gel Sci Technol 2005;34:77.
[23] Nair CPR, Glouet G, Guilbert Y. Polym Degrad Stab 1989;26:305.
[24] Yu Z, Zhang Z, Yuan Q, Ying S. Adv Polym Technol 2002;21:268.
[25] Yu YY, Chen CY, Chen WC. Polymer 2003;44:593.